Shape-Controlled Platinum Nanocubes and Their Assembly into Two-Dimensional and Three-Dimensional Superlattices

ARTICLE *in* THE JOURNAL OF PHYSICAL CHEMISTRY B · OCTOBER 2008

Impact Factor: 3.3 · DOI: 10.1021/jp802081n · Source: PubMed

5 AUTHORS, INCLUDING:

Arnaud Demortiere
French National Centre for Scientific Resea…
36 PUBLICATIONS **649** CITATIONS
SEE PROFILE

Pascale Launois
French National Centre for Scientific Resea…
140 PUBLICATIONS **2,205** CITATIONS
SEE PROFILE

Nicolas Goubet
Pierre and Marie Curie University - Paris 6
28 PUBLICATIONS **552** CITATIONS
SEE PROFILE

Christophe Petit
Pierre and Marie Curie University - Paris 6
79 PUBLICATIONS **3,865** CITATIONS
SEE PROFILE

Shape-Controlled Platinum Nanocubes and Their Assembly into Two-Dimensional and Three-Dimensional Superlattices†

A. Demortière,‡ P. Launois,§ N. Goubet,‡ P.-A. Albouy,§ and C. Petit*,‡

Laboratoire des Matériaux Mésoscopiques et Nanométriques, UMR 7070, Université Pierre et Marie Curie-Paris 6, 4 place Jussieu 75252 Paris Cedex 05, France, and Laboratoire de Physique des Solides, UMR CNRS 8502, bât. 510, Université Paris Sud, 91405 Orsay Cedex, France

Received: March 10, 2008

Liquid−liquid phase transfer has been used to synthesize platinum nanocrystals with a cubic morphology. By finely tuning the parameters controlling the nucleation and growth processes, nanometric truncated cubes or perfect cubes may be obtained. To our knowledge, this is the first time such shapes are obtained with this procedure. The importance of both the length of the capping agent to control the growth process and the bromide anions as poison for the {111} facet is shown. The low degree of size polydispersity allows these nanocrystals to self-assemble with a long-range ordering in two-dimensional and three-dimensional supracrystals. According to the nanocrystal shape, simple cubic or face-centered cubic supracrystals are observed. It is remarkable to notice that well-faceted supracrystals with sizes on the order of 10 μm may be obtained.

1. Introduction

The synthesis of nanocrystals with well-controlled shapes is of great interest to improve their individual and collective properties. The shape is a major factor in determining the specific properties in catalysis,[1] optics,[2] and magnetism.[3,4] For example, a change in the catalytic activity of platinum nanocrystals has been shown to coincide with a modification of their shape.[5] Indeed, the catalysis effect depends on the facets, edges, and corners of the nanocrystal.[6] The emergence of new methods to design magnetic nanocrystals such as nanocubes,[7–10] nanorods,[11–13] and cigar-shaped rods[14] has allowed the tuning of specific individual magnetic properties, such as, for example, the orientation of the magnetic easy axis and the shape anisotropy.[15] On the other hand, assembling the nanocrystals into long-range ordered suprastructures requires both a narrow size distribution and a uniform shape.[16] It is further well-known the lattice point symmetries must be compatible with those of the elementary unit. It is thus expected that the supracrystal structure will be dependent upon the shape of the nanocrystals acting as the elementary building blocks.[17] The synthesis of nanocrystals with original morphologies should thus lead to new long-range ordered structures and opens up the possibility of inducing specific collective properties.

Several techniques have been used to control the growth of nanocrystals with anisotropic shapes: growth in colloidal templates,[18,19] growth by selective-adsorption,[20] growth in the presence of external fields,[21] and seeded growth.[22] The classical model to understand the morphology of crystals is given in the framework of the Gibbs−Curie−Wulff theorem,[23] which dictates that the external equilibrium shape corresponds to the minimum surface energy for a given volume. However, several results revealed recently that, in complex systems such as colloidal systems, this purely thermodynamic argument cannot explain the shape evolution.[24] For instance, adsorption theory and kinetic models must also be taken into account. Thus, a new general framework should be established to describe all parameters governing the growth mechanisms.

In this variety of nanocrystal morphologies, the cubic shape is of interest because of its peculiar symmetries and the specific superstructures that may be associated with them.[25] In a pionnering work on nanocubes, El-Sayed et al.[26–30] reported the formation of Pt cubic nanocrystals (11 nm) using the reduction of a platinum salt ($PtCl_4^{2-}$) by H_2 in the presence of polyacrylate. Synthesis of silver nanocubes (100 nm) using a polyol method has been reported by Xia et al.[31,32] Other chemical methods based on organometallic decomposition have been used to obtain Fe,[12] FePt,[33] and $FePt_3$[10] nanocubes. In past years, a number of synthetic routes have been developed to produce a large variety of nanocubes, including such compounds as CeO_2,[34] PbSe,[35] PbS,[36] In_2O_3,[37] Co_30_4,[38] Fe_2O_3,[9] Fe_3O_4,[39,25] Pd,[40] Au,[41] and Ag.[42] Recently, the synthesis of platinum nanocrystals with different morphologies presenting the cubic symmetry has been reported.[43] However, the process used, based on the decomposition of an organometallic precursor at high temperature and under high hydrogen pressure, is not very convenient.

In this paper, we describe the first utilization of the liquid−liquid phase transfer method[44] to synthesize platinum with an overall cubic symmetry and a narrow size distribution. A study of the main parameters governing the synthesis mechanism has been carried out in order to understand their specific role. Long-range two-dimensional (2D) or three-dimensional (3D) self-assemblies are observed, whose superlattices depend on the specific shape of the elementary nanocrystals. These supracrystals, which are micrometricly large, display well-faceted morphologies. This can be related to the growth process, which is either homogeneous or heterogeneous.

2. Experimental Section

Chemicals. All products and solvents were purchased from a variety of sources and used without purification: hydrogen hexachloroplatinate (IV) hydrate (H_2PtCl_6) (Aldrich, 99,9%);

† Part of the "Janos H. Fendler Memorial Issue".
* To whom correspondence should be addressed.
‡ Université Pierre et Marie Curie.
§ Université Paris Sud.

10.1021/jp802081n CCC: $40.75
Published on Web 09/26/2008

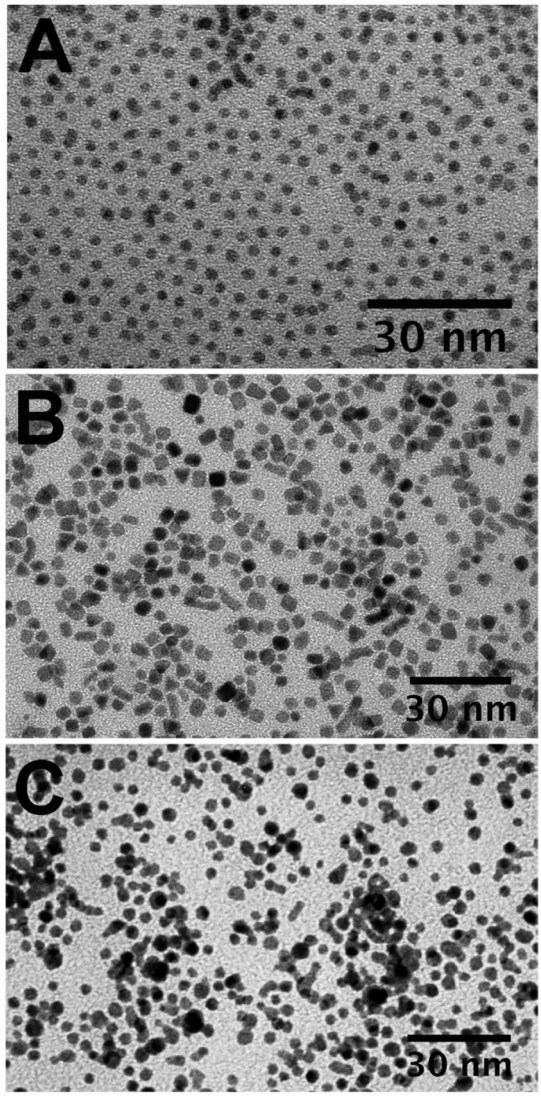

Figure 1. TEM images of platinum nanocrystals by adding the capping agent (A) before the reducing agent, (B) 45 min after introducing the reducing agent, and (C) 45 min after introducing the reducing agent but in open air.

tetrakis(decyl)ammonium bromide (TDAB), tetrakis(octyl)ammonium bromide (TOABr), tetrakis(octyl)ammonium chloride (TOACl), and sodium borohydride ($NaBH_4$), heptylamine ($C_7H_{15}NH_2$) (Aldrich,99%); hexadecylamine ($C_{16}H_{33}NH_2$) and octylamine ($C_8H_{17}NH_2$) (Fluka, 99%); dodecylamine ($C_{12}H_{25}NH_2$) (Fluka, 99,5%). Water was purified with a Millipore system (18.2 MΩ). After synthesis, the nanocrystals were stored under nitrogen in a glovebox.

Transmission Electron Microscopy (TEM) Measurements. An electron microscope JEOL 1011 (100 kV) with magnifications up to 500 000 was used to obtain TEM images and selected area electron diffraction (SAED) images; the camera length could be increased to 250 cm to operate in small-angle conditions. Samples were prepared by allowing one drop of a solution of nanoparticles in toluene to evaporate under ambient conditions on a TEM grid. High-resolution TEM (HRTEM) images were obtained with an HRTEM JEOL 2010 operating at an acceleration voltage of 200 kV (LaB_6).

Scanning Electron Microscopy. The morphology of superlattices grown from nanocube solutions was visualized using a scanning electron microscope (SEM) JEOL 5510LV.

Small-Angle X-ray Diffraction. X-ray diffraction experiments were performed with a rotating anode generator operated with a small focus (copper anode, wavelength: $\lambda = 0.15418$, focus size: 0.2×0.2 mm^2, power: 50 kV, 20 mA). The optics consisted of two parabolic multilayer graded mirrors at right angles. It delivers a well-defined and intense parallel monochromatic beam. The sample was mounted on a rotation stage, and the diffraction patterns were recorded onto photostimulable imaging plates. Vacuum pipes were inserted between the sample and the imaging plate to reduce air scattering. We used grazing incidence geometry, and the sample was allowed to oscillate by a few degrees during exposure.

3. Synthesis of Platinum Nanocubes

A liquid−liquid phase transfer method was used to synthesize platinum nanocrystals, similar to that described in a previous publication concerning CoPt nanocrystals.[45] However, some modifications have been brought to the procedure. In the classical Brust method, the reducing agent is added in the presence of the coating agent (alkylamine) in the biphasic solution. One method to increase the nanocrystal size is to introduce a delay between the beginning of the reduction step and the addition of the coating agent;[46] this is the route presently followed.

All the different reaction steps were performed in a glovebox under nitrogen. The platinum complex solution ($PtCl_6[TDA]_2$, $C = 1.55 \times 10^{-3}$ mol·L^{-1}) was prepared from an aqueous stock solution of $PtCl_6^{2-}$ added to a toluene solution of TDAB ($C = 2 \times 10^{-2}$ mol.L^{-1}). The quaternary ammonium serves as transfer agent of the metallic salt from the aqueous to the toluene fraction. After complete phase transfer, the aqueous phase was separated and discarded. The platinum organic solution was added to 20 mL of toluene, and an aqueous solution of $NaBH_4$ (0.1 mol·L^{-1}) was slowly added under rapid magnetic stirring. After 45−180 min of aging time, the coating agent (alkylamine) was introduced. This delay is presently defined as the ripening time (τ_{rip}) and is discussed later. After overnight stirring (ca. 16 h), the organic and aqueous phases were finally separated.

Extraction of the Nanocrystals. The platinum nanoparticles were recovered by evaporation of the organic solution using a rotary evaporator. The residual paste was divided into four, and an excess of ethanol was added; then the nanocrystals were precipitated by centrifugation. This sequence allows us to discard the supernatant containing the excess of octylamine and reaction byproduct. This procedure was repeated three times, and finally the colloids were dispersed into 4 mL of toluene. To eliminate unstable nanocrystals in the solution, a last centrifugation was performed. The supernatant was collected for further investigation.

4. Control of the Shape of the Platinum Nanocrystals

Effect of the Experimental Conditions on the Platinum Nanocrystals. It is quite difficult to control the size and the shape of the nanocrystals using the liquid−liquid phase transfer.[44,46,47] Post-treatments such as germination process,[46] digestive ripening,[48] or heat treatment[49] are often proposed to increase the particle size. Allowing the solution to age prior to the addition of the agent could be an alternative way, as it has been demonstrated in the case of gold.[50] Figure 1f shows the platinum nanocrystals obtained by adding octylamine before (Figure 1A) and 45 min after (Figure 1B) introduction of the reducing agent. In the first case, the presence of the capping agent prior the addition of the reducing agent avoid nuclei growth, then spherical nanocrystals with an average diameter of 2 nm are observed. In the second case, the nuclei are allowed to grow in the synthetic batch before the addition of the capping agent, then triangular and cubic nanocrystals with an average

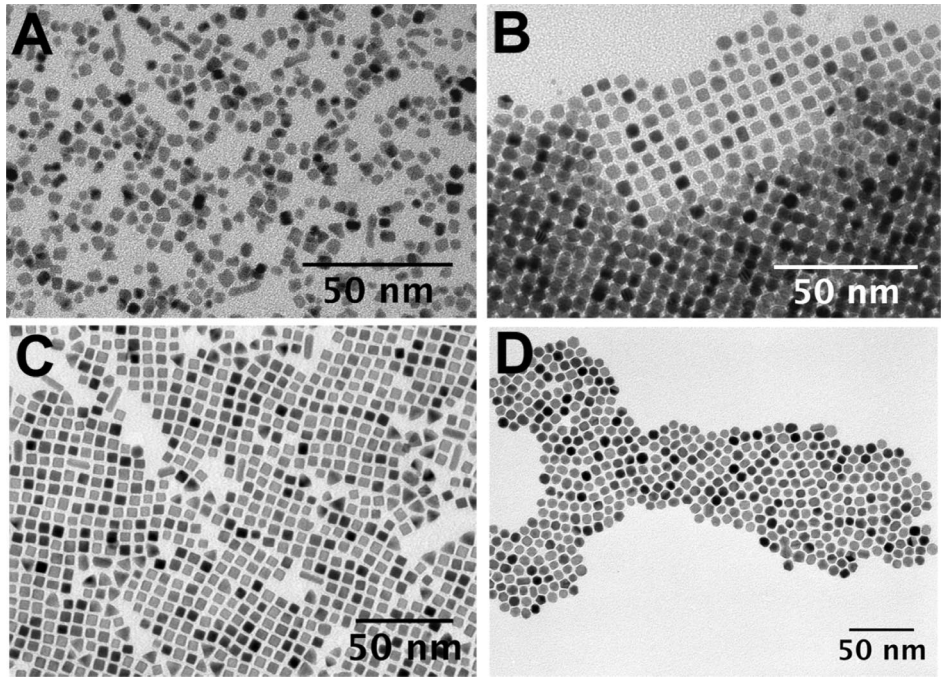

Figure 2. TEM images of platinum nanocrystals synthesized for ripening times of (A) 45 min, (B) 90 min, (C) 120 min, and (D) 180 min.

TABLE 1: Structural Parameters of Platinum Nanocrystals Depending on the Ripening Time and the Alkylamines Chains

ripening time (min)	alkylamine chains	average size (nm)	polydispersity (%)	cubic shape (%)
0	C8	2	10	0
45	C8	4.3	12	60
90	C8	4.7	8	87
120	C8	5.5	6	90
180	C8	6.7	5	40
120	C16	2.3	26	0
120	C12	3.2	13	10
120	C7	5.2	7	86

size of 4.3 nm are obtained. Indeed, the formation of anisotropic nanocrystals as observed here is rather remarkable in the case of the liquid−liquid phase transfer method because it usually leads to quasi-spherical nanoparticles.[47] Figure 1C shows the platinum nanocrystals obtained in open air. Oxygen appears to affect the growth process drastically as nanocrystals are now not clearly faceted and are highly polydisperse in size; some coalescence could also be observed. This suggests a surface perturbation of the platinum nanocrystals, which is probably related to the strong affinity of oxygen with platinum, as indicated by its action in fuel cell catalysis. In fact, specific interaction of O_2 with small platinum clusters has been reported.[51] It can be supposed that the adsorption of oxygen on the nanocrystal surface diminishes the ability of TDAB to bind to it. In these conditions, the passivation effect of TDAB is lowered, which may lead to uncontrolled growth.

Influence of the Ripening Time. The formation of large gold nanocrystals by increasing the ripening time has previously been reported.[49] Following a similar approach, we have increased the ripening time (τ_{rip}) from 45 to 180 min; in each case, the reaction is stopped 16 h after alkylamine addition. The final morphology of nanocrystals obtained for the different durations is well-illustrated by the TEM images given in Figure 2. As expected, the average size increase from 4.3 to 6.7 nm with a decrease of the size polydispersity (Table 1). However, a surprising shape evolution is obtained as the nanocrystals appear more and more cubic: polydisperse in shape at τ_{rip}= 45 min (Figure 2A), truncated cubes at τ_{rip} = 90 min (Figure 2B), and then perfect cubes at τ_{rip} = 120 mn, where 90% of the nanocrystals are perfectly cubic (Figure 2C). The average size is 5.5 nm with a size polydispersity of 6%. Further increase of τ_{rip} yields an increase in the average size of well-faceted nanocrystals but without shape uniformity (Figure 2D).

Influence of the Alkylamine Coating Agent. It is expected that the nature of the coating agent should play a role in the final state of the nanocrystals. In the case of gold nanocrystals, it has been observed that the final size is inversely dependent on the binding strength of the ligand.[50] We have shown in the case of platinum and CoPt that the interfacial rigidity also plays an important role concerning the size of the inorganic nanocrystals obtained by liquid−liquid phase transfer.[45,52] Following these lines, alkylamines with different chain lengths were tested as the final capping agent, using a similar ripening time in all cases (120 min). The resulting particles are shown in Figure 3, and the corresponding data are collected in Table 1. It is shown that, for longer alkylamin chains, $C_{16}H_{33}NH_2$ (Figure 3A), no shape control and no evolution of the average size of the nanocrystals is obtained compared to the case where the capping agent is added prior to the reducing agent, whereas a huge polydispersity is observed. Conversely, using short alkylchains, $C_8H_{17}NH_2$ (Figure 3C) or $C_7H_{15}NH_2$ (Figure 3D), the shape of the nanocrystals is cubic (nearly 90%), with a larger average size (about 5.5 nm) and a very small size polydispersity. If faceting would develop during the ripening time, it should be observed in all cases. This clearly demonstrates that faceting as well as particle growth happen in the presence of the coating agent. In the work of Saunders et al. on gold nanocrystals, a size increase was reported with increasing ripening time without shape effect.[49]

Discussion on the Growth Mechanism. At the beginning of the reduction step, which corresponds to the introduction of $NaBH_4$, TDAB molecules act as labile capping agents that stabilize the platinum nuclei by reducing the interfacial energy. The binding between this protective ligand and the platinum

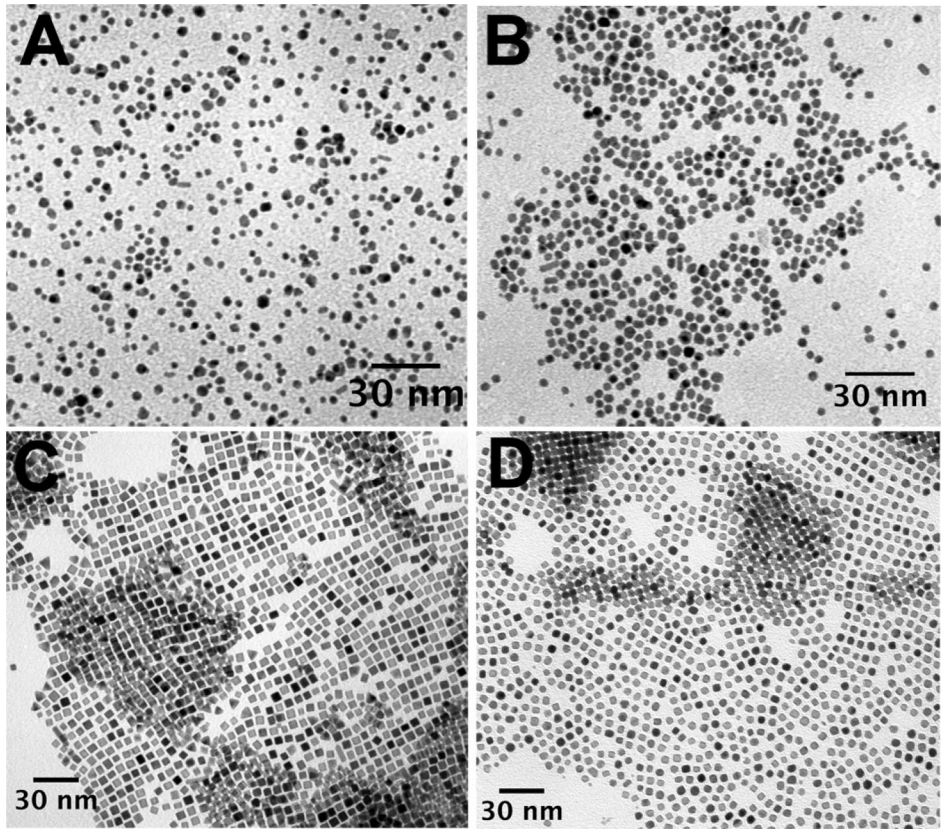

Figure 3. TEM images of platinum nanocrystals synthesized for different alkylamines: (A) hexadecylamine, (B) dodecylamine, (C) octylamine, and (D) heptylamine (ripening time 120 mn).

surface is electrostatic in nature and considered weak.[48] This configuration is expected to favor further crystal growth by allowing easy access to the particle surface.[49] Thus, it is not doubtful that the introduction of the coating agent after the ripening time will drastically slow down the growth process as a result of its stronger bonding ability. From this point of view, the effect of the alkylamine chains may seem surprising, considering that the strength of the interaction with the metal surface, which is mediated by the amino group, should be the same for all alkylamines. In fact, the particle size effect may be explained by a lower solubility in toluene of alkylamines with longer chains, which favors their adsorption at the particle interface.[52] The coating layer is thus expected to be not only thicker but also denser when using longer-chain alkylamines. Such a palisade will reduce the access of new platinum−TDAB complexes to the particle surface, resulting in smaller average sizes. This sterical hindrance is expected to be maximal with the C16 alkylamine, in which only spherical particles with an average size of 2.3 nm occur (Figure 3A). In this condition, the nanocrystal growth is prevented, and the final size and shape are not very different from those in the case where the reducing agent is added prior to the capping agent. This strongly suggests that the determination of the nanocrystal shape depends on the growth of the seed during the following step (maturation time), where both the capping agent and the TDAB molecules are present for 16 h under stirring in the same batch prior to the extraction. Thus TDAB should play a role. The effect of ions acting as a poisoning agent of specific crystalline facets is often reported; it induces an anisotropic growth, yielding specific shape.[53,54] In particular, the cetyltrimethylammonium bromide (CTAB) surfactant is usually used to obtain shape-specific gold[55] or silver[56] nanocrystals. Ab initio calculations of the optimal morphology of face-centered cubic (fcc) particles generally take into account only the denser {111} and {100} surfaces. Pure {100} faceting gives cubic shapes, whereas {111} and {100} faceting yields octahedrons. The equilibrium shape is normally between both faceting types. It has been previously reported that bromide anions have a high affinity for {100} facets.[30,53,54] Thus, the TDAB surfactant, which is present in excess at the beginning of the synthesis, acts as a labile coating agent that prevents coalescence and stabilizes the nanoparticles in solution. Fink et al.[46] have shown that, for gold nanocrystals synthesized by Brust's method, Br^- anions are adsorbed on the crystal and induced an electrostatic adsorption site, allowing the TDA^+ molecules to passivate the nanoparticles. A similar configuration can be assumed in our case. To prove the influence of the counterion on the growth process, bromide and chloride tetraalkylammoniums have been used as phase transfer agents at the same concentration: 7.5×10^{-2} mol·L^{-1} (TOABr and TOACl). The reactions have been carried out using octylamine as the final coating agent and $\tau_{rip} = 120$ min. TEM images displayed in Figure 4 the nanoparticles synthesized in the presence of TOABr (Figure 4A) and TOACl (Figure 4B). The nanocrystals obtained in the presence of bromide have clearly faceted morphologies and are nearly cubic (inset of Figure 4A). In contrast, the use of chloride generates elongated and heterogeneous morphologies (inset of Figure 4B). Indeed, the preferential adsorption of bromide on {100} facets will favor the fixation of TDA^+ species and hence will hinder the growth of the nanocrystals in the {100} direction. Thus {111} facets are expected to grow more rapidly and will have a tendency to disappear, leading to cubic crystals.

The above results suggest the following mechanism. During the first stage of the reaction, the nuclei growth takes place in the presence of the weakly binding TDAB surfactant. Compared with the usual conditions, the absence of the alkylamine, which

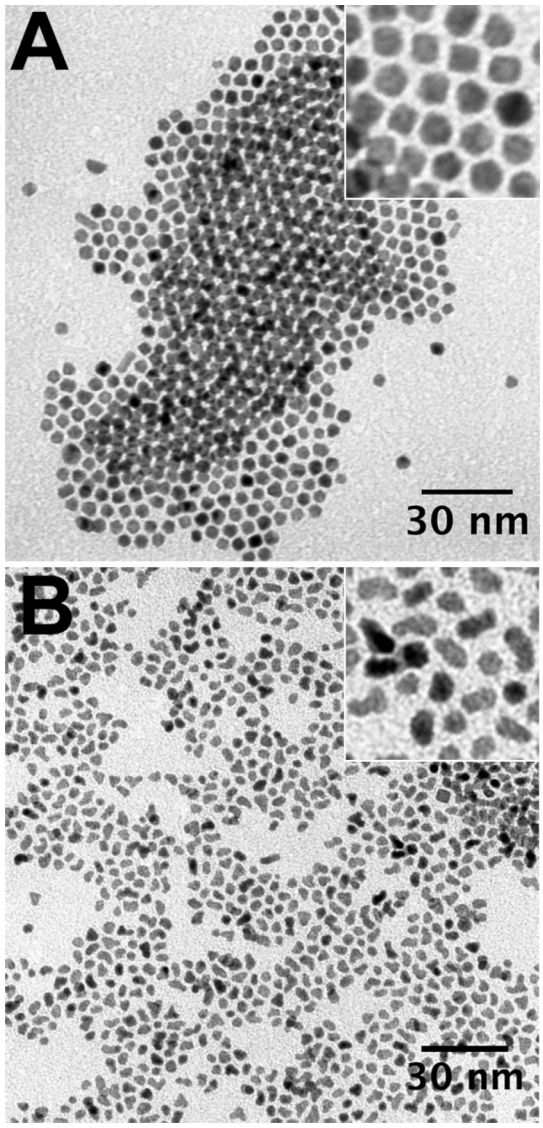

Figure 4. TEM images of platinum nanocrystals synthesized from (A) TOABr and (B) TOACl.

blocks the growth of the nuclei, during the initial reduction favors a seed-growing mechanism. Then, after the nucleation stage, the crystalline phase and the initial shape of the nuclei are determined. Consistent with our results, we can assume single-crystal truncated octahedral in fcc structure is the shape of nuclei. This has been observed, when alkylamine is added under similar experimental conditions, prior to the reducing agent.[52] Then the growth is initiated during the ripening time, and the seeds grow until the facets become large enough to bond the capping materials. Whether this process is achieved depends on the ripening time. Afterward, the injection of the alkylamine causes a growth slow down for the shorter chains and a growth stop for the longer chains. The combined action of the TDAB, which orientates the growth of the {111} facets and the octylamine, which slows the growth mechanism, is the key to the platinum nanocube synthesis. Nevertheless, it is important to note that, if the TDAB concentration ($C = 2 \times 10^{-2}$ mol·L^{-1}) in the solution increases significantly (2−3 times), then the Pt nanocrystals do not have a specific cubic shape but a spherical shape. Thus, there is a maximum concentration for the formation of the anisotropic shape. Indeed, in his works on AgBr nanoparticles,[56] Sugimoto demonstrated that the variation of bromide concentration changed the growth

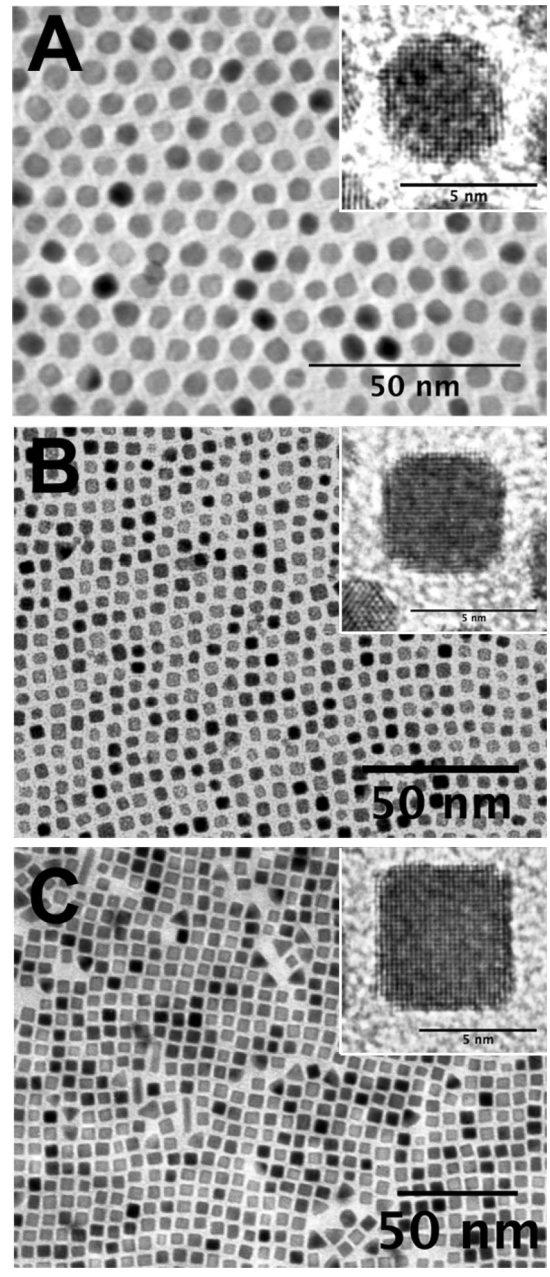

Figure 5. TEM images of platinum nanocrystals self-organized in a hexagonal network (A) ($\tau_{rip} = 60$ min), a quasi-square network (B) ($\tau_{rip} = 90$ min), and a square network (C) ($\tau_{rip} = 120$ min). HRTEM images are given in the insets. Deposition conditions: amorphous carbon-coated TEM grids, single-drop deposition at a concentration of 1×10^{-4} mol·L^{-1}.

rate of the {100} and {111} faces. Moreover, we can assume that, according to the [Br$^-$], the growth regime changes from thermodynamic growth with a diffusion-controlled mode to kinetic growth with a reaction-controlled mode. In this last regime, the nanocube formation is favorable because the growth rates of the {100} and {111} faces are different. Here, although the final shape is likely to be kinetically driven, the growth rate depends on many parameters, and the determination of the growth regime is not easy. On the basis of studies of varying the accessible growth parameters, we have discovered the critical factors in the formation of Pt nanocubes.

5. Self-Organization in 2D and 3D Superlattices

2D Self-Assemblies. As it is well-known, self-assemblies of nanocrystals require low size and shape polydispersity.[57] The

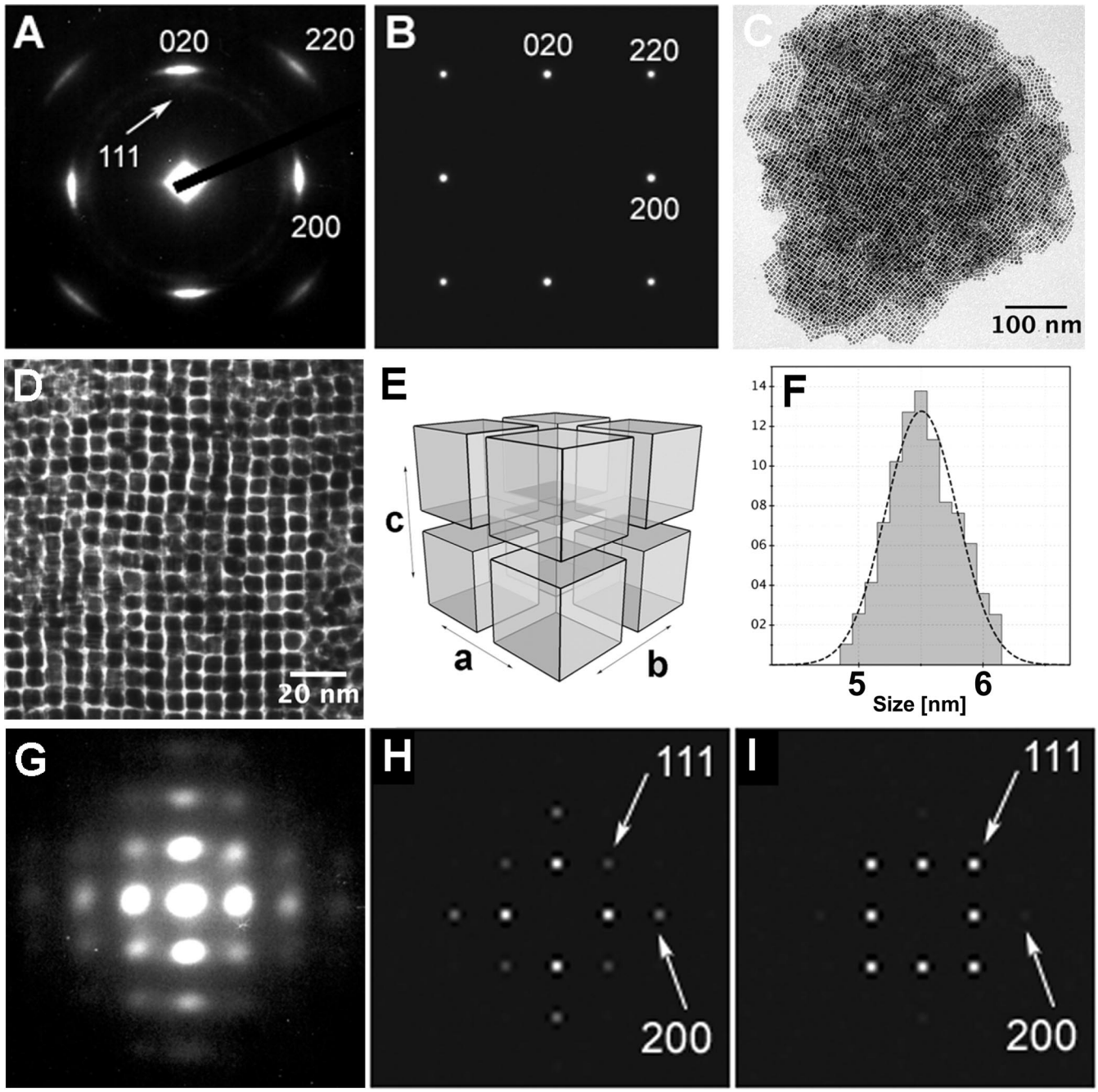

Figure 6. Cubic nanocrystals. (A) Wide-angle SAED pattern. (B) Numerical simulation of A. (C,D) TEM images of self-assembled superlattices. (E) Scheme of cubic superlattices of nanocubes. (F) Size distribution. (G) Small angle. (H,I) Numerical simulation of the small-angle SAED.

organization results mainly from an equilibrium between the attractive van der Waals forces and the repulsive steric forces.[58] As these forces are isotrope, this yields, for spherical nanocrystals, a 2D hexagonal pattern.[57,58]

The elaboration of 2D and 3D superlattices is generally performed by controlled evaporation of the organic solvent from small polydisperse nanocrystal suspensions in the presence of a deposition substrate. A large variety of ordered structures in 2D and 3D macroscopic assemblies have been observed this way.[57–63] Here the self-assemblies are obtained by drop deposition of platinum nanocrystal solution on TEM grids coated by an amorphous carbon film. As the colloidal nanocrystals have a narrow size distribution, they spontaneously self-assemble in 2D monolayers (Figure 5). As expected, a hexagonal pattern is observed for nearly spherical particles, (Figure 5A, $\tau_{rip} = 60$ min). For cubic nanocrystals (Figure 5C, $\tau_{rip} = 120$ min), the TEM image clearly reveals a square lattice made of platinum nanocubes. In the case of truncated cubes (Figure 5B, $\tau_{rip} = 90$ min), long-range order is not well-defined. In fact, a transition occurs between the hexagonal pattern and the quadratic pattern. This transition is due to the truncature of the nanocrystals, which are not totally spherical in shape, as in Figure 5A, nor cubic, as in Figure 5C. This shows that the arrangement mechanism is dependent on the crystal shape. This could indeed be expected from the fundamental rules of crystallography that stipulate that the object and lattice symmetries must be compatible. Here, the change of the nanocrystal shape is accompanied by a gradual increase in the {100} face surface compared to the {111} face, which favors a face-to-face attachment forming a high interdigitation bond.[63] The increase of the interaction between particles with their cubicity is clearly demonstrated by the variation of the interparticle distances: the interparticle distance

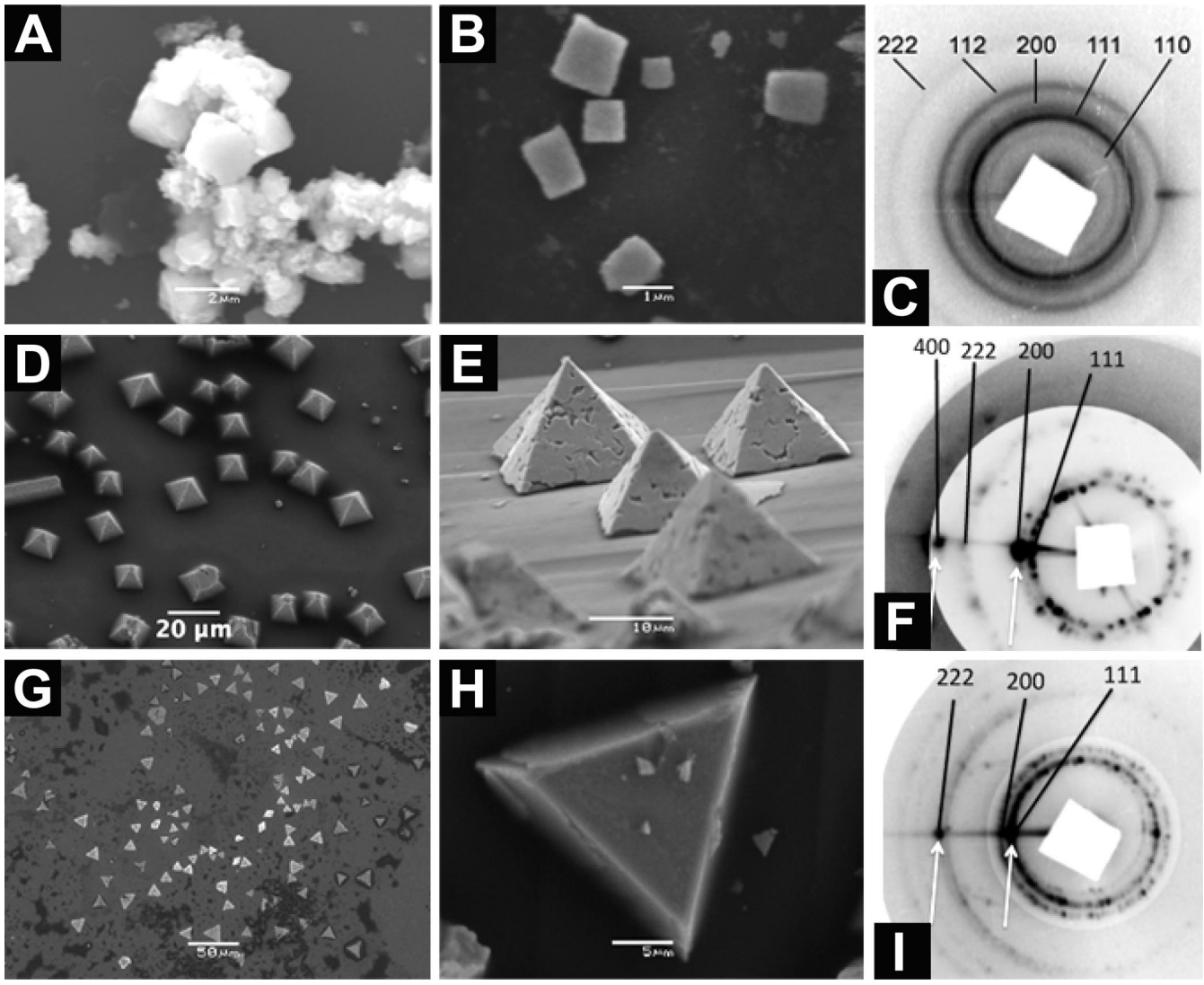

Figure 7. (A,B) SEM images of superlattices in cubic shape obtained with platinum nanocubes. (C) Corresponding X-ray diffraction pattern. (D,E) SEM images of superlattices in pyramidal shape obtained with truncated nanocubes. (F) Corresponding X-ray diffraction patterns. (G,H) SEM images of superlattices in triangular shape obtained with truncated nanocubes. (I) Corresponding X-ray diffraction pattern of the superlattices.

is 3 nm (border to border) for quasi-spherical particles, which corresponds to twice the length of fully extended octylamine (1.5 nm length). It is 2.6 nm for truncated cubes and 2 nm for cubes. The increase of the interaction between the {100} faces thus induces chain interdigitation and a higher compacity of the network.

3D Supracrystals. It should be noted that the dropwise deposition method induces defect in the monolayers, as observed in Figure 5C, where the presence of triangular or elongated nanocrystals partly induces defect in the self-assembly. This can be avoided by using an immersion process where the substrate is immersed in a solution of nanocrystals, which slowly evaporate under controlled atmosphere. In this condition, a spontaneous segregation process occurs during the self-assembly process, which excludes nanocrystals having strong deviation from the average size and shape.[60,61] Hence, 3D superlattices of cubic and truncated cubic nanocrystals have been grown by close control of the evaporation conditions (Figures 6–8). For this purpose, 200 μL of colloidal solution ($C_j = 2 \times 10^{-5}$ mol·L^{-1}) are slowly evaporated (12 h) in a glass container with substrate (TEM copper grid coated by amorphous carbon) placed at the bottom. We also show that micrometer-sized single supracrystals can be build from nanoparticle solutions (Figure 7). For this purpose, the technique of controlled evaporation of a carrier solvent (toluene) from the nanocrystal solution allows us to obtain organized structures with a high degree of long-range ordering.[60] A volume of 2 mL ($C = 2 \times 10^{-5}$ mol·L^{-1}) of colloidal solution was slowly evaporated (8 days) on a silicon wafer (5 × 5 mm) placed on the bottom of a glass container of cylindrical geometry (1 × 5 cm) at room temperature.

Case of Cubic Nanocrystals ($\tau_{rip} = 120'$). The 3D structures obtained by the self-assembly of nanocubes were first investigated by TEM (Figure 6). Panels C and D of Figure 6 are direct images obtained at different magnifications and reveal the organization of the 5.5 nm cubic nanocrystals (see histogram of size in Figure 6F) in well-ordered superlattices. A square-like arrangement is observed in Figure 6D. The order was checked by SAED, measured at wide- and small-angles, and is respectively shown in Figure 6A,G (camera lengths of 80 and 250 cm, respectively). Wide-angle diffraction peaks (Figure 6A) originate from the scattering by individual nanocrystals, while small-angle ones (Figure 6G) are associated with their ordering in a "superlattice". Numerical simulations of the diffraction patterns are presented in Figure 6B,H,I. They have been computed within the kinematical approximation, and they are

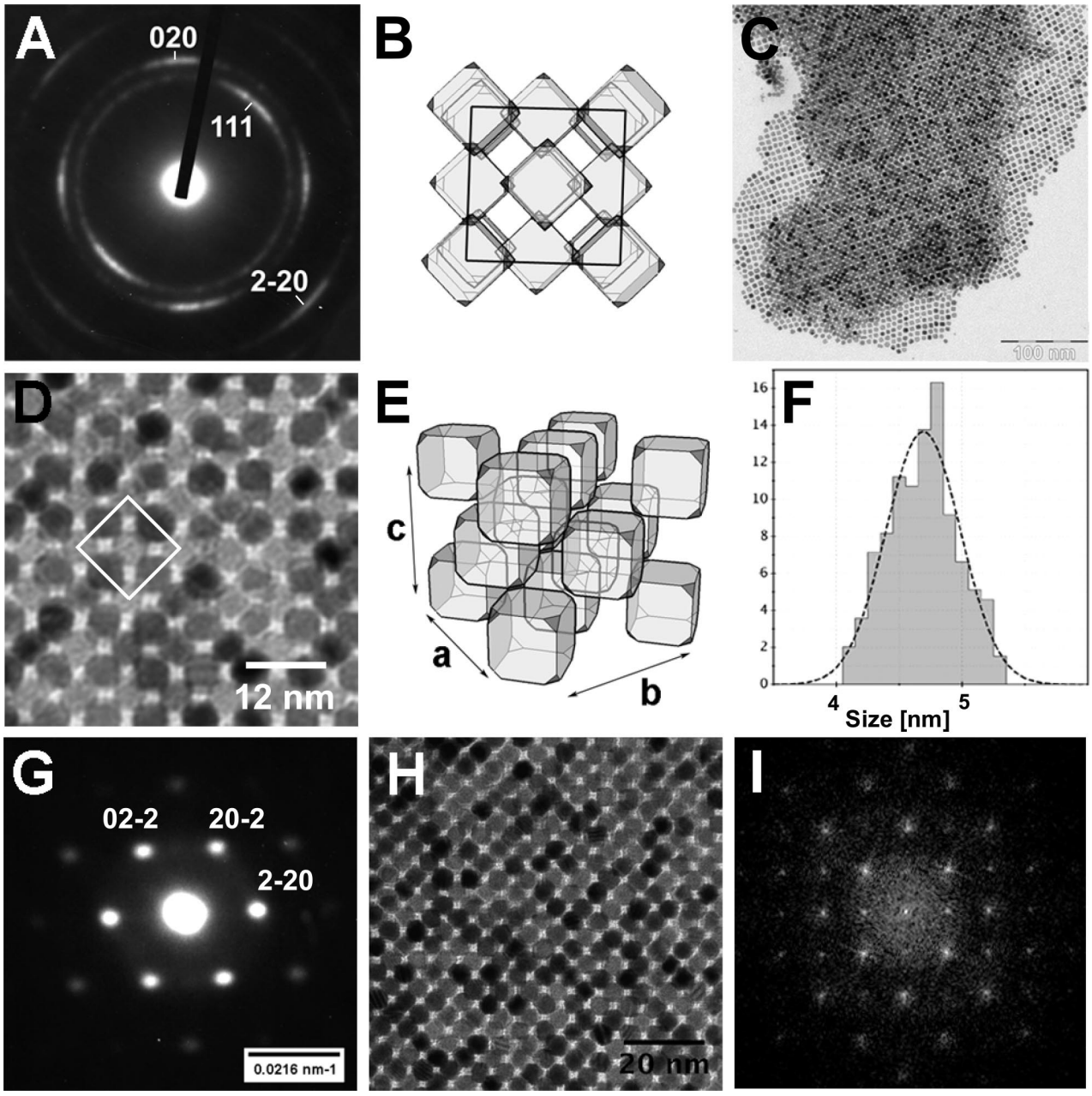

Figure 8. Truncated cubic nanocrystals. (A) Wide-angle SAED pattern. (C,D) TEM images of self-assembled superlattices. (B,E) Picture showing the nanocubes positions into the fcc superlattices. (F) Size distribution of the truncated nanocubes. (G) SAED at small angle with a tilt of 30°. (H) Superlattice with the 4-fold symmetry. (I) Fourier transform of the picture in H.

TABLE 2: Data Table of Small Angle X-ray Diffraction: Experimental and Calculated Coordinates of Diffraction Spots Assuming a Simple Cubic Structure (Cubic Shape)

Q measured [Å^{-1}]	Q calculated [Å^{-1}]	h	k	l
0.115	0.115	1	1	0
0.141	0.140	1	1	1
0.163	0.162	2	0	0
0.202	0.199	1	1	2
0.283	0.280	2	2	2

TABLE 3: Data Table of Small Angle X-ray Diffraction: Experimental and Calculated Coordinates of Diffraction Spots Assuming an fcc Structure

Q measured [Å^{-1}]	Q calculated [Å^{-1}]	h	k	l
0.0985	0.0988	1	1	1
0.1139	0.1140	2	0	0
0.1622	0.1613	2	2	0
0.1893	0.1891	3	1	1
0.1970	0.1975	2	2	2
0.2279	0.2281	4	0	0

simply intended as a guide for the interpretation of the experimental data.

The wide-angle diffraction pattern in Figure 6A clearly presents 4-fold symmetry. The calculated pattern in Figure 6B is obtained assuming that the nanocrystals possess the fcc structure of bulk platinum (unit cell parameter 0.392 nm), their [001] axis being parallel to the electron beam. It follows that the observed peaks in Figure 6A correspond to the (200) and (220) reflections of the platinum nanocrystals. The angular width of the (200) reflections is 10°, indicating a weak disorientation of the nanocrystals, one with respect to the other. Indeed the TEM image in Figure 6D shows that nanocrystal faces are only parallel in average from a nanocrystal to its neighbor, with some fluctuation in orientation being allowed. Very weak additional

diffraction rings, corresponding to the {111} and {200} planes, can also be seen, corresponding to a small fraction of strongly misorientated nanocrystals.

The surprising square shape of the central spot observed in Figure 6A is simply the blurred image of the small-angle diffraction pattern shown in Figure 6G. The superlattice can be indexed as a primitive cubic, with parameters $a = b = 6.6$ nm (Figure 6E), in agreement with the TEM image in Figure 6D. This result is not surprising, as a primitive cubic lattice corresponds to the dense packing of cubic units (the Wigner−Seitz cell of a primitive cubic being a cube). Numerical calculations have been performed to show, within the kinematical approximation, the influence of the nanocrystal shape on the reflection intensity. The diffraction patterns (Figure 6H,I) have been calculated with a form factor equal to the Fourier transform of a cube that assumes that all nanocubes are in the same orientation (Figure 6H) and with a form factor equal to the Fourier transform of a sphere that assumes that the nanocubes are in a random orientation (Figure 6I). A comparison with the experimental diagram supports the first hypothesis, in agreement with Figure 6D. The orientational relationship between the Pt nanocrystal lattice and the superlattice is thus $[001] \parallel [001]_s$.

Let us now consider 3D supracrystals obtained using the procedure described above. SEM observations show supracrystals of cubic shape that are either grouped (Figure 7A) or isolated on the substrate (Figure 7B). Their typical lateral size is in the range 0.5−2 μm. A structural analysis has been carried out by small-angle X-ray diffraction in grazing angle geometry. The diffraction pattern obtained under these conditions (Figure 7C) shows homogeneous diffraction rings that correspond to randomly oriented supracrystals. As indicated in Table 2, the position of the diffraction rings is well accounted for using a simple cubic lattice of parameter $a = 8.19$ nm. The difference of the value extracted from TEM data ($a = 6.6$ nm) may be due to incertitude of the camera length of the electron microscope and/or to the scale of the supracrystals, which can be relaxed compared to the multilayers observed by TEM.

Case of Truncated Cubic Nanoparticles ($\tau_{rip} = 90'$). The data obtained by TEM are summarized in Figure 8. The wide-angle diffraction pattern in Figure 8A exhibits three diffraction rings associated with the (111), (200), and (220) reflections of the fcc platinum structure. Intensity reinforcements of the (200) ring clearly display 4-fold symmetry showing preferential alignment of the 100 and 001 axes of the nanocrystals. The observation of two (111) reflections could be explained either by a misorientation of part of the superlattice or disorientation of the truncated nanocubes in the organized structure or by a combination of both effects. It is likely that the truncation of nanocubes permits a greater misorientation of nanocrystals than in the case of perfect nanocubes. A TEM image of the superlattice is given in Figure 8B,C. A close examination reveals a square lattice corresponding to an fcc structure, as drawn in Figure 8B,E with a lattice parameter equal to 11 nm. Attempts to obtain correct diffraction images of this zone failed because of misorientation of the carbon grid. By tilting the sample, the diffraction pattern presented in Figure 8G could be obtained. It clearly shows that the system has 3- or 6-fold symmetry. This combined with the 4-fold symmetry of the image presented in Figure 8H and its Fourier transform (Figure 8I) indicates that the superlattice has cubic symmetry. This is consistent with the fcc structure assumed above.

Single supracrystals have been grown from solutions of truncated cubes using the above-described technique. SEM images reveal either pyramids with a square base (Figure 7 D,E) or truncated tetrahedral morphology (Figure 7 G,H). The typical size of these single crystals is in the range 5−30 μm. Both morphologies are compatible with 3- and 4-fold symmetries, as expected. In the case of pyramids, the angle between the normal to the substrate and the normal to the faces is close to 55°. X-ray diffraction patterns reveal punctuated diffraction rings (Figure 7F). The two dark spots (white arrows) correspond to the Bragg reflection associated with the main orientation (200). This is compatible with flat-lying (100) surfaces and (111) pyramid faces. For the truncated tetrahedra (Figure 7G,H), the diffraction pattern is given in Figure 7I. Two dark spots are also observed (white arrows) and correspond to the Bragg reflection associated with the main orientation (111). This is compatible with flat lying (111) surfaces and (100) faces of the tetrahedra. In both cases, the ring radii are perfectly accounted for, with an fcc lattice of parameter $a = 11.02$ nm (see Table 3), which is compatible with the TEM data of the superlattices. The punctuation of the rings depends upon the substrate area that is looked at. Simulations show that most single crystals have their (100) surface flat-lying for Figure 7D,E (pyramid), while Figure 7G,H corresponds mainly to the (111) orientations (some low-intensity reflections correspond to a small-proportion of crystals with flat-lying (220) surfaces (elongated structure on the left of Figure 7D)). These two majority orientations correspond to both morphologies seen by SEM.

Therefore, from these results, it is possible to connect the underlying structure of the nanocrystals to the supercrystal morphology. Furthermore, information can be deduced from the growth process of the supracrystals. The nanocrystal superlattice crystallization occurs either by heterogeneous nucleation on the substrate or by homogeneous nucleation in solution. The evaporation conditions determine the crystallization kinetics. However, a small variation in interparticle attractions leads to important changes in superlattice nucleation and growth kinetics.[64] In the case of truncated nanocubes, the nucleation seems to be heterogeneous because the structures are supported on the substrate; as a consequence, the diffraction patterns reveals strong punctuated diffraction rings. Conversely, for the nanocubes, the nucleation seems to be homogeneous because the superlattices are in a random position on the substrate; consequently, diffraction patterns reveal only homogeneous rings. This can be explained by the difference of the interparticle attraction forces during the solvent evaporation between the nanocube sample and the truncated nanocube sample. As shown above, the face-to-face van der Waals interactions appear stronger in the case of nanocubes, as a result of the perfect cubic shape. We can assume that this effect is sufficient to induce a modification of the nucleation mode, and thus favors homogeneous nucleation for the nanocubes and then permits the formation of cubic superlattices in solution. For truncated nanocrystals, the growth is induced by the substrates and then they start a specific 2D arrangement such as cubic (see Figure 5), yielding the pyramidal shape, or, for a minority part, they start from a 2D hexagonal arrangement yielding the triangular shape. Hence the shape of the nanocrystals controls the growth process of the supracrystal and thus the shape of the supracrystals.

Summary

For the first time, the liquid−liquid transfer method has been used to synthesize cubic nanocrystals of platinum. The role of a ripening time between the beginning of reduction and the introduction of a stable ligand (octylamine) that stops the reaction is clearly demonstrated. The optimal condition for nanocube synthesis corresponds to a ripening time of 120 min.

Spherical particles are obtained at ripening times of less than 60 min, with intermediate ripening times leading to truncated cubic shapes. Moreover, the action of TDAB seems to be necessary to induce a specific cubic shape: this is attributed to a poisoning effect of bromide anions on the {111} facets of particles. According to the shape of the nanocrystals, different supraorganizations are observed at two and three dimensions. In the case of truncated nanocubes, an fcc structure is obtained, while pure nanocubes self-assemble on a primitive cubic lattice. Most remarkable is the observation of well-faceted supracrystals with sizes on the order of 10 μm.

Acknowledgment. We would like to acknowledge Prof. J. H. Fendler for the well-founded criticism and council he gave to this work during his numerous stays in the LMZN at Paris 6. Moreover, he always treated people with great humanity. C.P. would like to personally acknowledge Prof. Fendler for everything he did for him.

References and Notes

(1) Feldheim, D.L. *Science* **2007**, *316*, 699.
(2) Eychmuller, A. *J. Phys. Chem. B* **2001**, *104*, 6514.
(3) Sun, S.; Murray, C. B.; Weller, D.; Folks, L.; Moser, A. *Science* **2001**, *291*, 2115.
(4) Chen, M.; Kim; J.; Liu, J. P.; Fan, H.; Sun, S. *J. Am. Chem. Soc.* **2006**, *128*, 7132.
(5) Narayanan, R.; El-Sayed, M.A. *J. Am. Chem. Soc.* **2004**, *126*, 7194.
(6) Huynh, W. U.; Dittmer, J. J.; Alivisatos, A.P. *Science* **2002**, *295*, 2425.
(7) Dumestre, F.; Chaudret, B.; Amiens, C.; Renaud, P.; Fejes, P. *Science* **2004**, *303*, 821.
(8) Wang, C.; Daimon, H.; Lee, Y.; Kim J.; Sun, S. *J. Am. Chem. Soc.* **2007**, *129*, 6974.
(9) Wang, S.-B.; Min, Y.-L.; Yu, S.-H. *J. Phys. Chem. C* **2007**, *111*, 3551.
(10) Margeat, O.; Tran, M.; Spasova, M.; Farle, M. *Phys. Rev. B* **2007**, *75*, 134410.
(11) Puntes, V. F.; Krishnan, K. M.; Alivisatos, A. P. *Science* **2001**, *291*, 2115.
(12) Dumestre, F.; Chaudret, B.; Amiens, C.; Respaud, M.; Fejes, P.; Renaud, P.; Zurcher, P. *Angew. Chem., Int. Ed.* **2003**, *42*, 5213.
(13) Aslam, M.; Bhobe, R.; Alem, N.; Donthu, S.; Dravida, V. P. *J. Appl. Phys.* **2005**, *98*, 074311.
(14) Ngo, A. T.; Pileni, M.-P. *J. Appl. Phys.* **2002**, *92*, 4649.
(15) Lee, H. K.; Schulthess, T. C.; Brown, G.; Landau, D. P.; Sorge, K. D.; Thompson, J. R. *J. Appl. Phys.* **2003**, *93*, 7047.
(16) Pileni, M. P. *J. Phys. Chem. C* **2007**, *111*, 9019.
(17) Song, Q.; Ding, Y.; Wang, Z. L.; Zhang, Z. J. *J. Phys. Chem. B* **2006**, *110*, 25547.
(18) Lisiecki, I. *J. Phys. Chem. B* **2005**, *109*, 12231.
(19) Pileni, M.-P. *Nat. Mater.* **2003**, *2*, 145.
(20) Peng, Z. A.; Peng, X. G. *J. Am. Chem. Soc.* **2001**, *123*, 1389.
(21) Wang, J.; Zeng, C. *J. Cryst. Growth* **2004**, *270*, 729.
(22) Murphy, J.; Sau, T. K.; Gole, A. M.; Orendorff, C. J.; Gao, J.; Gou, L.; Hunyadi, S. E.; Li, T. *J. Phys. Chem.* **2005**, *109*, 13857.
(23) Mullin, J. W. In *Crystallization*; Butterworth-Heinemann: Woburn, MA, 1997.
(24) Peng, Z. A.; Peng, X. G. *J. Am. Chem. Soc.* **2001**, *123*, 1389.
(25) Zheng, R.; Gu, H.; Xu, B.; Fung, K. K.; Zhang, X.; Ringer, S. P. *Adv. Mater.* **2006**, *18*, 2418.
(26) Ahmadi, T. S.; Wang, Z. L.; Green, T. C.; Henglein, A.; El-Sayed, M. A. *Science* **1996**, *272*, 1924.
(27) Ahmadi, T. S.; Wang, Z. L.; Henglein, A.; El-Sayed, M. A. *Chem. Mater.* **1996**, *8*, 1161.
(28) Wang, Z. L.; Petroski, J. M.; Green, T. C.; El-Sayed, M. A. *J. Phys. Chem. B* **1998**, *102*, 6145.
(29) Petroski, J. M.; Green, T. C.; El-Sayed, M. A. *J. Phys. Chem. A* **2001**, *105*, 5542.
(30) Nikoobakht, B.; El-Sayed, M. A. *Chem. Mater.* **2003**, *15*, 1957.
(31) Petrova, H.; Lin, C.-H.; de Liejer, S.; Hu, M.; McLellan, J. M.; Siekkinen, A. R.; Wiley, B. J.; Marquez, M.; Xia, Y.; Sader, J. E.; Hartland, G. V. *J. Chem. Phys.* **2007**, *126*, 094709.
(32) Im, S. H.; Lee, Y. T.; Wiley, B.; Xia, Y. *Angew. Chem., Int. Ed.* **2005**, *44*, 2154.
(33) Shukla, N.; Liu, C.; Roy, A. G. *Mater. Lett.* **2006**, *60*, 995.
(34) Yang, Z.; Zhou, K.; Liu, X.; Tian, Q.; Lu, D.; Yang, S. *Nanotechnology* **2007**, *18*, 185606.
(35) Lu, W.; Fang, J.; Ding, Y.; Wang, Z. L. *J. Phys. Chem. B* **2005**, *109*, 19219.
(36) Zhou, G.; Lu, M.; Xiu, Z.; Wang, S.; Zhang, H.; Zhou, Y.; Wang, S. *J. Phys. Chem. B* **2006**, *110*, 6543.
(37) Lee, C. H.; Kim, M.; Kim, T.; Kim, A.; Paek, J.; Lee, J. W.; Choi, S.-Y.; Kim, K.; Park, J.-B.; Lee, K. *J. Am. Chem. Soc.* **2006**, *128*, 9326.
(38) Xu, R.; Zeng, H. C. *J. Phys. Chem. B* **2003**, *107*, 926.
(39) Xiong, Y.; Ye, J.; Gu, X.; Chen, Q.-W. *J. Phys. Chem. C* **2007**, *111*, 6998.
(40) Chang, G.; Oyama, M.; Hirao, K. *Acta Mater.* **2007**, *55*, 3453.
(41) Jin, R.; Egusa, S.; Scherer, N. F. *J. Am. Chem. Soc.* **2004**, *126*, 9900.
(42) Yu, D.; Yam, V. W.-W. *J. Am. Chem. Soc.* **2004**, *126*, 13200.
(43) Ren, J.; Tilley, R. D. *J. Am. Chem. Soc.* **2007**, *129*, 3287.
(44) Brust, M.; Bethell, D.; Schiffrin, D. J.; Kiely, C. J. *Adv. Mater.* **1995**, *7*, 795.
(45) Demortière, A.; Petit, C. *Langmuir* **2007**, *23*, 8575.
(46) Fink, J.; Kiely, C. J.; Bethell, D.; Schiffrin, D. J. *Chem. Mater.* **1998**, *10*, 922.
(47) Brust, M.; Bethell, D.; Kiely, C. J.; Schiffrin, D. J. *Langmuir* **1998**, *14*, 5425.
(48) Cheng, W.; Wang, E. *J. Phys. Chem. B* **2004**, *108*, 24.
(49) Saunders, A. E.; Sigman, M.B., Jr.; Korgel, B. A. *J. Phys. Chem. B* **2004**, *108*, 193.
(50) Brust, M.; Fink, J.; Bethell, D.; Schiffrin, D. J.; Kiely, C. *J. Chem. Soc., Chem. Commun.* **1995**, 165.
(51) Wang, Z. L.; Gao, R. P.; Nikoobakht, B.; El-Sayed, M. A. *J. Phys. Chem. B* **2000**, *104*, 5417.
(52) Wikander, K.; Petit, C.; Holmberg, K.; Pileni, M.-P. *Langmuir* **2006**, *22*, 4863.
(53) Filankembo, A.; Giorgio, S.; Lisiecki, I.; Pileni, M.-P. *J. Phys. Chem. B* **2003**, *107*, 7492.
(54) Jun, Y.-W.; Lee, J.-H.; Choi, J.-S.; Cheon, J. *J. Phys. Chem. B* **2005**, *109*, 14795.
(55) Sugimoto, T. *J. Colloid Interface Sci.* **1983**, *91*, 51.
(56) Sugimoto, T. *J. Colloid Interface Sci.* **1983**, *93*, 461.
(57) Motte, L.; Billoudet, F.; Pileni, M. P. *J. Phys. Chem.* **1995**, *99*, 16425.
(58) Motte, L.; Billoudet, F.; Lacaze, E.; Douin, J.; Pileni, M.-P. *J. Phys. Chem. B* **1997**, *101*, 138.
(59) Wang, Z. L. *Adv. Mater.* **1998**, *10*, 13.
(60) Lisiecki, I.; Albouy, P.-A.; Pileni, M.-P. *Adv. Mater.* **2003**, *15*, 712.
(61) Courty, A.; Albouy, P. A.; Mermet, A.; Duval, E.; Pileni, M. P. *J. Phys. Chem. B* **2005**, *159*, 21.
(62) Taleb, A.; Petit, C.; Pileni, M. P. *Chem. Mater.* **1997**, *9*, 950.
(63) Wang, Z. L. *Mater. Charact.* **1999**, *42*, 101.
(64) Sigman, M. B.; Saunder, A. E.; Korgel, B. A. *Langmuir* **2004**, *20*, 978.

JP802081N